International Journal of Advanced Research in Chemical Science (IJARCS)
Volume 4, Issue 4, 2017, PP 1-10
ISSN 2349-039X (Print) & ISSN 2349-0403 (Online)
http://dx.doi.org/10.20431/2349-0403.0404001
www.arcjournals.org

Synthesis of Composite Oxides Derived from Zn-Ni-Al Layered Double Hydroxides and its Use in Photocatalytic Reduction of CO_2

Li ZHANG, Qing-man LIANG, Jian-hui YAN, Min-jie ZHOU

College of Chemistry and Chemical Engineering, Hunan Institute of Science and Technology, Yueyang China

Abstract: *$ZnO/NiO/ZnAl_2O_4$ mixed metal oxides were synthesized through a facile and environment-benign route in which solutions of appropriate amounts of metal salts were mixed with solutions of sodium hydroxide and sodium carbonate to obtain a series of hydrotalcite-like precursors. The precursors in the form of ZnNiAl layered double hydroxides (LDHs) were subject to calcination at suitable temperatures for the generation of composite oxides. The as-obtained samples were characterized by XRD, SEM, TEM, EDS, BET and UV-Vis DRS techniques. The results indicate that there is the generation of well-crystalline ternary $ZnO/NiO/ZnAl_2O_4$ photocatalysts high in surface area. The photocatalytic activity of the as-obtained materials was evaluated in the photocatalytic reduction of CO_2 under simulated sunlight irradiation. The effects of calcination temperature, amount of sacrificial agent and reaction time on the photocatalytic activity of the samples were investigated. The results indicated that ZnNiAl-LDH precursor calcined at 500 °C show the highest photocatalytic activity, the maximum yield of 2680 umol·g_{cat}^{-1} methanol within 6 h was obtained with 0.04 mol of NaOH and Na_2SO_3, respectively. The mechanism of CO_2 photocatalytic reduction over $ZnO/NiO/ZnAl_2O_4$ was discussed.*

Keywords: *Layered double hydroxides; $ZnO/NiO/ZnAl_2O_4$; Photocatalytic reduction; CO_2*

1. INTRODUCTION

As a class of inorganic materials with special layered structure and interesting properties, layered double hydroxides (LDHs) photocatalysts have aroused more and more attention. Interlayer water molecules of LDH photocatalysts would be lost after calcination, and then the composite oxides with high specific surface area could be formed. Generally, the LDH photocatalysts are composed of amphoteric metal ions, such as Al^{3+} Zn^{2+} ions and so on [1,2]. Mesh-like mesoporous spinel compounds with large specific surface area can be obtained via the alkaline dissolution of LDH after calcination. Spinel amphoteric metal oxides can exhibit porous structure and high specific surface area, which is mainly attributed to the amphoteric materials. On the one hand, the amphoteric materials can play the role of dispersion and barrier, which can effectively inhibit the growth of spinel nanoparticles. On the other hand, the mesoporous structure can be obtained during the selective dissolution [3]. Currently, LDH derivatives mainly consisted of two or three metal composite oxides. Binary [4], ternary [5] or quaternary [6] metal ionic LDH compounds can be formed via the interactions among divalent or trivalent metal ions. In the ternary LDH photocatalysts, the ternary metal ions are able to enter into the layers of the hydrotalcite by several ways, and then trivalent complex oxide could be obtained after calcination [7, 8]. In addition, quaternary LDH composite can also be obtained through the metal oxide combination or noble metal deposition [9]. It has been reported that the nickel-based compound as co-catalyst is effective in improving the photocatalytic activity [10,11]. Gabriela Carja and coworkers prepared Ni/MgAl-LDH and Ni/MgFeAl-LDH photocatalysts by intercalating exchange method, which displayed high photocatalyst activity in degrading the Drimaren industrial dyes [12]. Kentaro Teramura group prepared fluorinated Ni/Al binary LDHs via co-precipitation approach, which could effectively converse CO_2 in water solution system under ultraviolet light [13]. Zn-Ni-Al complexes

were also prepared by co-precipitation method, which were used to reduce CO_2 and degrade methyl orange, and all of them showed remarkable properties [14, 15].

In this work, zinc, nickel, aluminum nitrate were used as the main raw materials to prepare the Zn-Ni-Al-LDH by hydrothermal method. The mixed oxides with high specific surface were obtained by the thermal treatment of LDH materials. The photocatalytic activity was evaluated by photocatalytic reduction of CO_2, and the factors influencing the photocatalytic activity were explored, such as calcination temperature, sacrifice dosage and reaction time.

2. EXPERIMENTAL

2.1. Sample Preparation

The hydrotalcite containing Zn-Ni-Al with different cationic ratios were prepared by hydrothermal method according to the reference [16]. A mixed metal nitrates with specific cationic molar ratio ($Zn^{2+}/Ni^{2+}/Al^{3+}$ = 2:1:1) was dissolved in deionized water to produce a solution with a total cationic concentration of 1 M (solution A); and NaOH and Na_2CO_3 were dissolved in deionized water to form a mixed alkali solution (solution B). The concentrations of the alkali were related to those of the metal ions as follows: $[CO_3^{2-}]$ = 1.8 $[Al^{3+}]$, $[OH^-]$ = 1.4 ($[Ni^{2+}]$ + $[Zn^{2+}]$ + $[Al^{3+}]$). The solution B was dropped at a rate of 0.05mL min^{-1} into solution A at 80 ^oC while stirring at a rate of 600 rpm. During the synthesis the pH value was kept at 9.0. The resulting slurry was aged for 1 h at 80^oC, transferred into a Teflon reaction kettle and incubated for 10 h at 150 ^oC. The final precipitates were recuperated by filtration, washed several times with deionized water and dried at 80 ^oC overnight. And then the resulting Zn-Ni-Al ternary LDH precursors were fully milled and calcined at different temperatures (400, 500, 600, and 700 °C).

2.2. Characterization

Powder X-ray diffraction data (XRD) were collected on a Rigaku D/max 2550 diffractometer under the following conditions: 40 kV, 300 mA, graphite-filtered Cu Kα radiation (λ = 0.15406 nm). The powder samples were step-scanned in steps of 0.04° (2θ) using a count time of 10 s /step. Scanning electron microscopy (SEM) and TEM images were recorded on Nova Nano230 and Tecna G220. The specific surface area determination and pore volume and size analysis were performed by BET (ASAP，2020，HD88，America) method. UV-vis absorbance spectra were recorded on a LS55 Perkin Elmer spectrometer (America). And the products of photocatalytic reduction were tested by gas chromatograph (GC-2010, Japan).

2.3. Photocatalytic Activity

The CO_2 reduction reaction was carried out in a quartz catalytic reactor (Xe lamp, 300 W). The photocatalyst (1.0 g•L^{-1}) was dispersed in deionized water in the reactor. The CO_2 was flowed into the reacted mixture at a flow rate of 200 mL min^{-1} at 25 ^oC. Meanwhile, different amounts of NaOH and anhydrous Na_2SO_3, as a sacrificial agent, were added and continuously stirred for 30 min. The reductive reaction started after turning on the light source. Subsequently, the reaction liquid was regularly extracted and post-processed while the content of methanol in the filtrate was detected by gas chromatograph.

3. RESULTS AND DISCUSSION

3.1. Characterization

3.1.1. XRD Analysis

Fig. 1 indicates the XRD patterns of ZnNiAl-LDH ($Zn^{2+}/Ni^{2+}/Al^{3+}$ = 2:1:1) precursors calcined at different temperature. The XRD patterns exhibit the characteristic peaks of layered double hydroxides with the basal peaks for (003), (006) and (009/012) planes and the non-basal peaks for (110) and (113) planes, which illustrate the good symmetry of LDHs crystal layer structure [17, 18]. Additional $Zn(OH)_2$ phase is present in the samples, showing intense and sharp peaks for (009) and (012) planes.

The reflections corresponding to LDH have completely disappeared and new reflections appear after calcination at 400-700 ◦C. The reflections become sharp with the increasing calcination temperature. The reflections at 2θ = 31.8°, 34.4°, 36.2°, 47.6° and 56.6° can be indexed to hexagonal wurtzite structured ZnO, which is in good agreement with the literature values (JCPDS 36-1451). In addition, the peak centering at 2θ = 43.3° and 62.8° in the XRD pattern can be associated with the NiO phase (JCPDS 36-1451). When calcined temperature was further increased, the reaction between oxides occurred and generated the spinel structure $ZnAl_2O_4$ [19]. When calcined temperature was increased to 500 ^oC, the reflections at 2θ = 36.9° can be indexed to $ZnAl_2O_4$ (JCPDS 05-0669) [20]. This may be ascribed to homogeneous distribution of metal cations within a single LDH precursor, which facilitates the formation of well-dispersed and crystalline mixed metal oxides through a topotactic process upon calcinations. When calcined temperature was further raised, the diffraction peak intensity is enhanced, indicating the increased crystallinity. While no diffraction peak of $NiAl_2O_4$ phase was found in all samples. The content of ZnO is higher than NiO in the mixture. Compared with $NiAl_2O_4$, $ZnAl_2O_4$ is easier to produce at relatively low temperatures. No characteristic reflections corresponding to Al_2O_3 phase can be observed, suggestive of the presence of amorphous Al_2O_3.

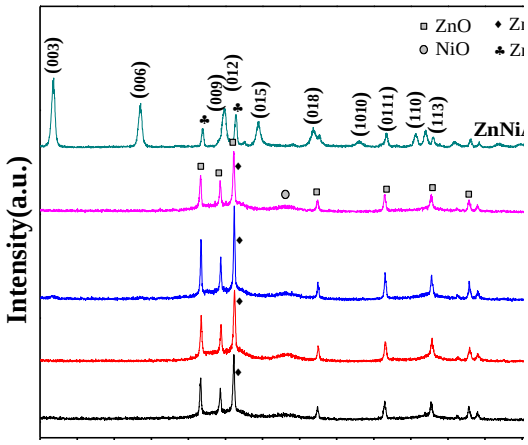

Fig1. *XRD patterns of Zn-Ni-Al-LDH and Zn-Ni-Al-LDHs calcined at different temperatures*

3.1.2. SEM and TEM Analysis

The SEM images of ZnNiAl-LDH before and after calcination are presented in Fig. 2. It can be seen that the precursor is made up of agglomerated platelet-like particles, and the platelets have a side length of 20-50 nm (Fig. 2a). After calcination at 500 °C, there is the collapse of LDH structure and the platelets become irregular spherical particles about 20 nm (Fig. 2b).

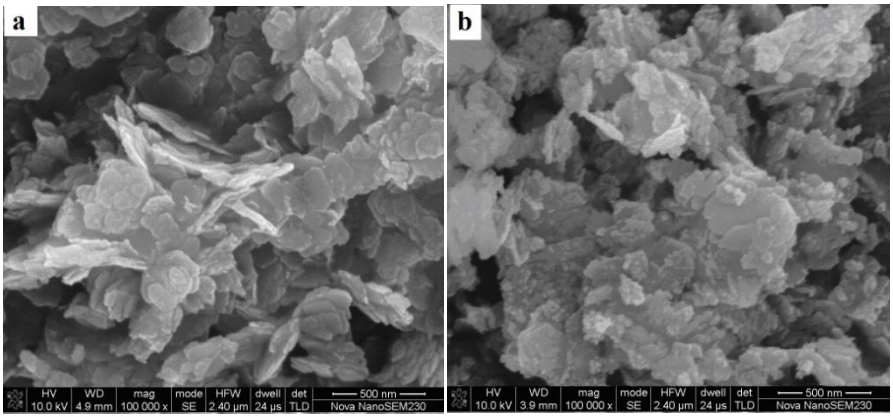

Fig2. *SEM images of (a) Zn-Ni-Al-LDH and (b) Zn-Ni-Al-LDH calcined at 500 ℃*

The TEM and HRTEM images of ZnNiAl-LDH before and after calcination are presented in Fig. 3. As shown in Fig. 3a, ZnNiAl-LDH possesses uniform distribution of LDH particles with some irregularly hexagon particles. In Fig. 3b, the average particle size of ZnNiAl-LDH decreases upon calcination at 500 °C to the formation of metal oxide cluster. The HRTEM image and EDX pattern of ZnNiAl-LDH calcination at 500 °C are presented in Figs. 3(c) and (d). The spacing of 0.281 nm and 0.237 nm depict the lattice-resolved (100) and (200) crystalline plane of ZnO and NiO phase, respectively, and the spacing value of 0.284 nm corresponds to the (220) facet of $ZnAl_2O_4$ phase (Fig. 3c). EDS measurement confirmed the presence of Zn, Ni, Al and O in the calcined sample (Fig. 3d).

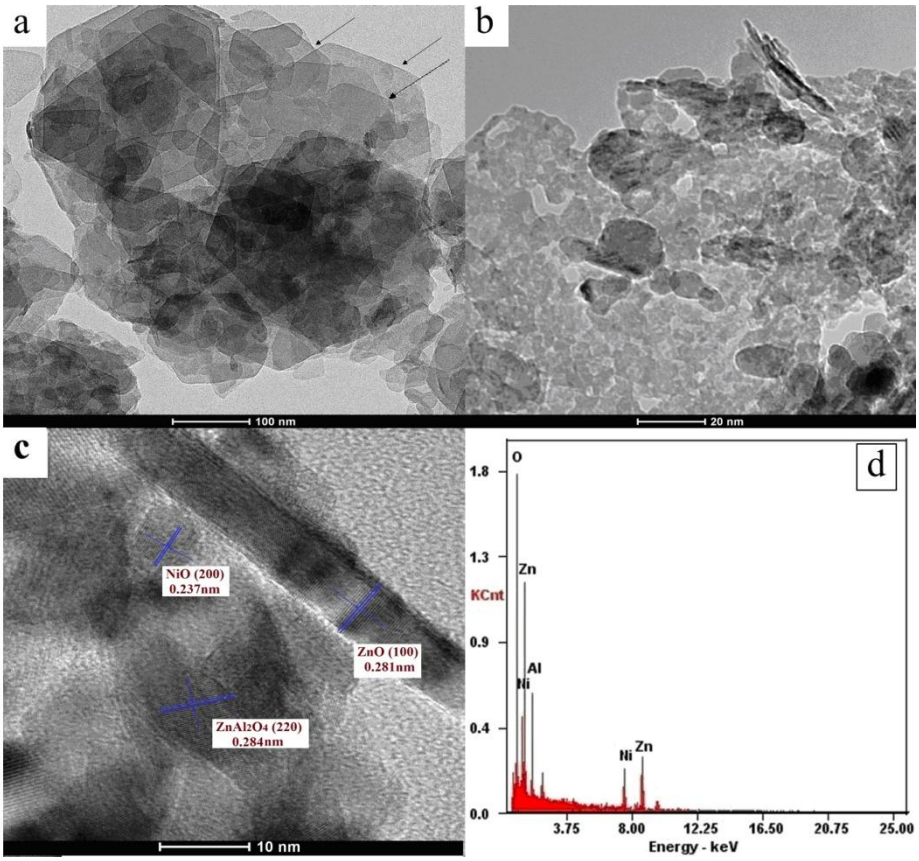

Fig3. *TEM images of (a) Zn-Ni-Al-LDH and (b) Zn-Ni-Al-LDH calcined at 500 ℃along with (c) HRTEM image and (d) EDS measurement of Zn-Ni-Al-LDH calcined at 500 ℃*

3.1.3. UV-Vis DRS Analysis

The UV–visible absorption spectra of ZnNiAl-LDH before and after calcination are depicted in Fig. 4a. The *Eg* values were also estimated based on the Kubelka-Munk equation [21]. Upon calcination, ZnO, NiO and $ZnAl_2O_4$ composite oxides (Fig. 1 XRD shown) coupled to each other to form a heterojunction (Fig. 3c HRTEM) that could reduce the bandgap energy and improve the light quantum efficiency while the absorption becomes intense and the absorption peak generates bathochromic shift [16].

$$F(R_\infty) = \frac{(1-R_\infty)^2}{2R_\infty} = \frac{\alpha}{S}$$

α is the absorption coefficient, *S* is the scattering coefficient, R_∞ is the diffuse reflectance.

The band gap of Zn-Ni-Al-LDHs is 5.45 eV, that is to say, hydrotalcite does not belong to the semiconductor material without light catalytic ability. Meanwhile the calcined sample has certain absorption in the visible area for the band gap of 3.1 eV.

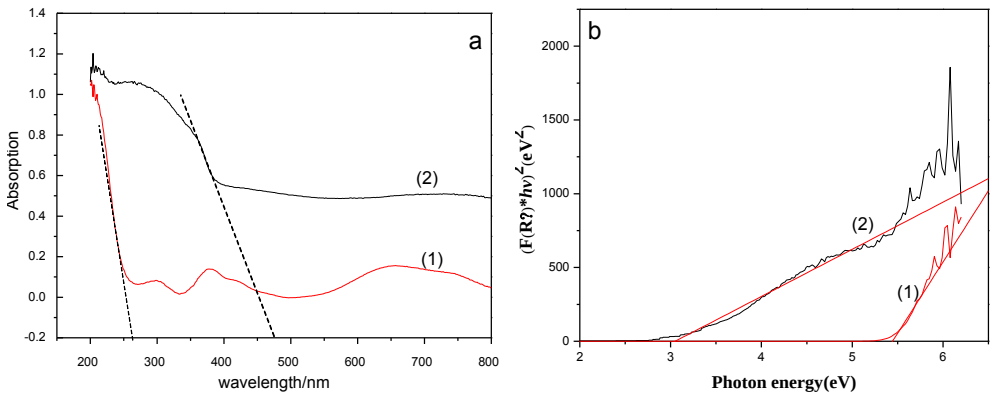

Fig4. *UV-Vis diffuse reflectance spectra （a）and band-gap energy (b) of (1) Zn-Ni-Al- LDHs and (2) Zn-Ni-Al-LDHs calcined at 500 ℃*

3.1.4. BET Surface Area and Pore Size Analysis

Table 1 shows the specific surface area and pore structure parameters of Zn-Ni-Al-LDHs precursor and calcined samples (400, 500 and 600 ℃). The specific surface area of the hydrotalcite precursor is about 73.8 $m^2 \cdot g^{-1}$, and the average pore size is up to 15.9 nm due to the pile layered structure, but the total pore volume is small, only 0.29 $cm^3 \cdot g^{-1}$, which shows the moderate number of holes in the sample. The specific surface area and pore volume of the calcined samples were increased obviously. Especially, the sample calcined at 500 ℃ has the specific surface area of 153.5 $m^2 g^{-1}$ that is 2.1 times high than unburned precursor. Such pore structure is more conducive to the photocatalytic reduction of CO_2 [22]. In parallel, calcination temperature was further increased, which caused the bonding among the oxide, and the specific surface area, pore volume and average pore diameter were reduced [3].

Table1. *BET and pore-structure data of Zn-Ni-Al-LDH and Zn-Ni-Al-LDH calcined at diffferent temperatures*

Sample number	Calcination temperature/ °C	S_{BET} / ($m^2 \cdot g^{-1}$)	Adsorption average pore width / nm	Pore volume / ($cm^3 \cdot g^{-1}$) (P_s/P_0 = 0.9918)
1	unfired	73.8	15.9	0.29
2	400	141.8	10.8	0.31
3	500	153.5	9.9	0.36
4	600	146.1	9.2	0.35

As a comparison in Figure 5, the calcinated sample has more porous structure, resulting in a significant hysteresis loop and the emergence of the adsorption platform at high P/P_0 ($0.9<P/P_0<1$) place in its N_2 adsorption-desorption curves [23]. According to pore size distribution of calcinated samples, the mesoporous regional distribution is more even and the pore volume is opposite greater, indicating that suitable calcination can lead to collapse of the laminate structure and water loss.

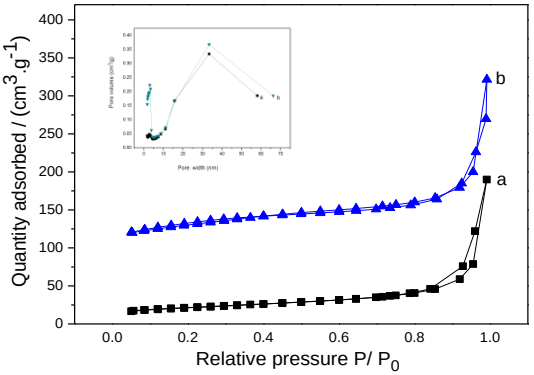

Fig5. *Nitrogen adsorption-desorption isotherms and pore size distribution curves of samples (a) Zn-Ni-Al-LDH (b) Zn-Ni-Al-LDH calcined at 500 °C*

3.2. Photocatalytic Activity

3.2.1. Effect of Calcination Temperature on the Photocatalytic Activity

Fig. 6 shows the effect of calcination temperature on the photocatalytic activity over the Zn-Ni-Al-LDHs calcined at 300, 400, 500, 600 and 700 °C. It was found that the catalytic efficacy was not linearly raised with temperature, and the maximum yield of methanol reached 2680 μmol·g $_{cat}^{-1}$ with the sample calcined at 500 °C, which could be explained by the structure of calcined samples. According to TEM and SEM results, the obtained composite after calcination at 500°C achieved the optimum conditions among the specific surface area, the degree of crystallinity and oxide composition ratio, making it has the highest photocatalytic reduction activity [24]. In other words, at different calcination temperatures, the hydrotalcite was converted into ZnO, NiO, $ZnAl_2O_4$ and $NiAl_2O_4$ in different proportions while multi-heterojunction structure was diverse [25].

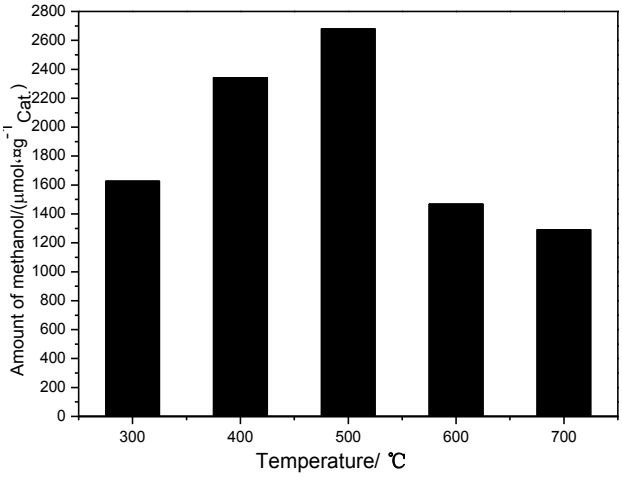

Fig6. *The influence of calcination temperature on methanol production*

3.2.2. Effect of Reduction Time on the Photocatalytic Activity

Photoreduction of CO_2 is a complex process. The reduction products contained HCOOHCO, HCHO, CH_3OH and CH_4. Even the amount of reduction for each product would change over time [26]. It should be noted that the maximum amount of methanol generated within 6 h, and then reduced in Figure 7. This is because the gradually increased electrons is conducive to the reaction in the initial reaction activation process until 6 h, the photo-generated electron-hole generation, separation and consumption balance and the amount of methanol reach optimum values. However, with the continued reaction progress, methanol was continuously produced and was further reduced to methane and other products, eventually, the total content of methanol declined.

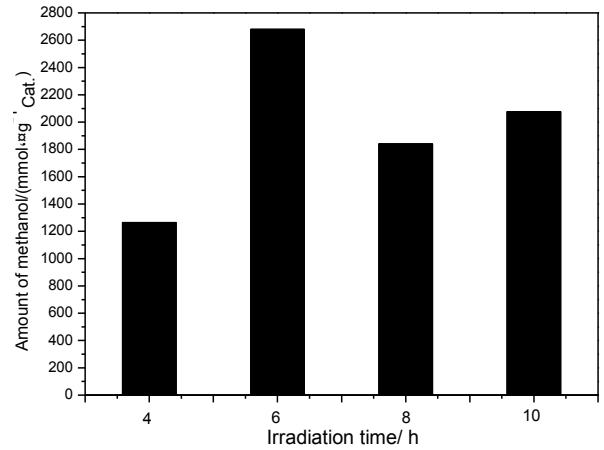

Fig7. *The influence of different reaction time on methanol production*

3.2.3. Effect of Sacrifice Dosage on the Photocatalytic Activity

Photocatalytic reduction processes with a continuous production and consumption of photo-generated electrons, need a charge balance to make the photocatalytic reaction continued, and otherwise the presence of the reverse potential will inhibit the further production of the photo-generated charge. It has been reported that the sacrificial agent can quickly eliminate the potential difference, thereby helping to generate photo-generated charge, while the positive charge timely consumption can reduce recombination of photoinduced charge to improve the quantum efficiency [27, 28]. In this study, Na_2SO_3 and NaOH using as sacrificial agent can help to dissolve CO_2, but also make the oxidation of SO_3^{2-} successfully completed under alkaline conditions. In this reaction system, as long as the valence band potential of the photocatalyst is higher than the price charged sulfate of 0.93 eV, the oxidation reaction can be carried out smoothly. As shown in Figure 8, different amounts of sacrificial agent influenced photoreduction of CO_2 within 6 h. It is obvious that the amount of NaOH and Na_2SO_3 is 0.04 mol, respectively, and the generation amount of methanol reaching a maximum value (2680 $\mu mol \cdot g_{cat}^{-1}$). However, when only NaOH or Na_2SO_3 was added, the generation amount of methanol was 1267 $\mu mol \cdot g_{cat}^{-1}$ or 1853 $\mu mol \cdot gcat^{-1}$, respectively. Compared with the expense of mixing agent, the amount of CH_3OH is greatly reduced. That is to say, sacrificial agent under basic conditions has a great impact on photoreduction activity [29].

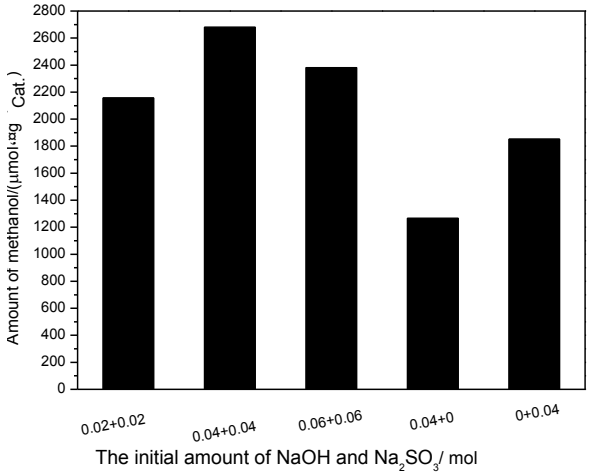

Fig8. *The influence of sacrificial agent amount on methanol production*

3.3. Mechanism Analysis of Photocatalytic Reaction

A schematic illustration about the photocatalytic mechanism is presented in Figure 9. Under the simulated sunlight, photo-generated electrons excited from the valence band to the conduction band and formed the corresponding holes (h^+) and free electrons (e^-), and then photo-generated charge migrated from the interior to the surface of the catalyst. When the compound semiconductor conduction band position is more negative than CO_2/CH_3OH potential (-0.38 eV) and the valence band position is more positive than SO_3^{2-}/SO_4^{2-} potential (0.93 eV), the photocatalytic reduction of CO_2 can be achieved. The ZnO, $ZnAl_2O_4$ and NiO conduction and valence bands were -0.31 eV, 2.89 eV，-1.14 eV, 2.66 eV and -0.50 eV, 3.0 eV, respectively. $ZnAl_2O_4$ can only be inspired by ultraviolet light and the resulting holes (h^+) and free electrons (e^-) easily compounded. When it forms a heterojunction with ZnO composite structure, $ZnAl_2O_4$ conduction band electrons migrate to the ZnO conduction band while the positive charge of ZnO valence band migrate to $ZnAl_2O_4$. In comparison, the composite oxides, containing ZnO, NiO and $ZnAl_2O_4$, have the lowest bandgap energy. In this case, the positive charge on the NiO can be further migrated to $ZnAl_2O_4$ valence band by ZnO valence band. That is to say, the introduction of NiO and the formation of composite oxide are beneficial for isolating photo-generated electric carriers, reducing the band gap energy and improving the reduction activity [30].

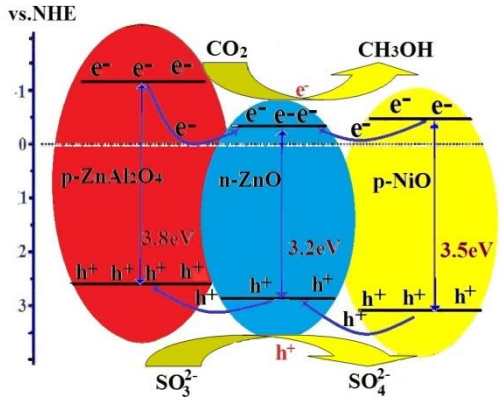

Fig9. *Mechanism illustration of photocatalytic reduction of CO_2 over $ZnO/NiO/ZnAl_2O_4$*

4. CONCLUSIONS

1) $ZnO/NiO/ZnAl_2O_4$ mixed-metal oxides with high BET surface area of 153.5 $m^2 \cdot g^{-1}$ were successfully synthesized through a hydrotalcite-like precursor route.
2) The mixed-metal oxide showed superior photocatalytic performance. A maximum of photocatalytic reduction of CO_2 was achieved from the LDH calcination at 500 °C.
3) The highest amount of methanol within 6 h reaches 2680 $umol \cdot g_{cat}^{-1}$ with 0.04 mol of NaOH and Na_2SO_3 as sacrificial agent, respectively.

ACKNOWLEDGMENTS

This research was financially supported by the National Natural Science Foundation of China (No. 51372080), the Natural Science Foundation of Hunan Provincial of China (No. 2017JJ2108), and the Scientific Research Foundation of Hunan Provincial Education Department of China (No. 15A076).

REFERENCES

[1] AHMED A A A, TALIB Z A, HUSSEIN M Z. Influence of sodium dodecyl sulfate concentration on the photocatalytic activity and dielectric properties of intercalated sodium dodecyl sulfate into Zn-Cd-Al layered double hydroxide [J]. Materials Research Bulletin, 2015, 62: 122-131.

[2] ABDERRAZEK K, NAJOUA F S, SRASRA E. Synthesis and characterization of [Zn-Al] LDH: Study of the effect of calcination on the photocatalytic activity [J]. Applied Clay Science, 2016, 119: 229-235.

[3] SEFTEL E M, POPOVICI E, MERTEN M, WITTE K D, TENDELOO G V, COOL P, VANSANT E F. Zn–Al layered double hydroxides: synthesis, characterization and photocatalytic application [J]. Microporous and Mesoporous Materials, 2008, 113(1): 296-304.

[4] PAUSOVA Š, KRYSA J, JIRKOVSKY J, FORANO C, MAILHOT G, PREVOT V. Insight into the photocatalytic activity of ZnCr–CO_3 LDH and derived mixed oxides. Applied Catalysis B: Environmental, 2015，170-171, 25-33.

[5] XIA Sheng-jie, ZHANG Lian-yang, ZHOU Xiao-bo, PAN Guo-xiang, NI ZHe-ming. The photocatalytic property for water splitting and the structural stability of CuMgM layered double hydroxides (M= Al, Cr, Fe, Ce)[J]. Applied Clay Science, 2015, 114: 577-585.

[6] Almeida M F D, Bellato C R, Mounteer A H, Ferreira S O，Milagres J L，Miranda L D L. Enhanced photocatalytic activity of TiO_2-impregnated with MgZnAl mixed oxides obtained from layered double hydroxides for phenol degradation[J]. Applied Surface Science, 2015, 357: 1765-1775.

[7] Miranda L D L, Bellato, C R, Milagres J L, Moura L G, Mounteer A H, Almeida, M F D. Hydrotalcite-TiO_2 magnetic iron oxide intercalated with the anionic surfactant dodecylsulfate in the photocatalytic degradation of methylene blue dye[J]. Journal of environmental management, 2015, 156: 225-235.

[8] ZHOU Yang-mei, LI Shuai, JIANG Xin-Yu, JIAO Fei-peng, YU Jin-gang. Visible-light-driven photocatalytic properties of layered double hydroxide supported-Bi_2O_3 modified by Pd (II) for methylene blue[J]. Advanced Powder Technology, 2015, 26(2): 439-447.

[9] SUN Jia-chao, ZHANG Yan-bing, CHENG Juan, FAN Hai, ZHU Jian-ying, WANG Xin., AI Shi-yun. Synthesis of Ag/AgCl/Zn-Cr LDHs composite with enhanced visible-light photocatalytic performance [J]. Journal of Molecular Catalysis A: Chemical, 2014, 382: 146-153.

[10] XU You, XU Rong. Nickel-based cocatalysts for photocatalytic hydrogen production[J]. Applied Surface Science, 2015, 351: 779-793.

[11] CANG Chi-jung, CHU Kuan-wu, HSU Mu-hsiang, CHEN Chin-yi. Ni-doped ZnS decorated graphene composites with enhanced photocatalytic hydrogen-production performance[J]. International Journal of Hydrogen Energy, 2015, 40(42): 14498-14506.

[12] CARJA G, HUSANU E, GHERASIM C, IOVU H. Layered double hydroxides reconstructed in $NiSO_4$ aqueous solution as highly efficient photocatalysts for degrading two industrial dyes[J]. Applied Catalysis B: Environmental, 2011, 107(3): 253-259.

[13] IGUCHI S, TERAMURA K, HOSOKAWA S. Photocatalytic conversion of CO_2 in water using fluorinated layered double hydroxides as photocatalysts[J]. Applied Catalysis A: General, 2016, 521: 160-167.

[14] LI Bing-jie, WU Zhi-jian, CHEN Shu, SHANGGUAN Wen-feng, YUAN Jian. Preparation and photocatalytic CO_2 reduction activity of Ni/Zn/Cr composite metal oxides[J]. Journal of Molecular Catalysis, 2014, 28: 268-274.

[15] YUAN Bing, ZHANG Xin, HOU Wang-guo. Synthesis of Zn–Ni–Al Layered Double Oxides and its Photocatalytic Property[J]. Journal of the Chinese Ceramic Society, 2012, 40(8):1184-1189(6).

[16] ZHAO Xiao-fei, WANG Lei, XU Xin, LEI Xiao-dong, XU Sai-long, ZJHANG Fa-zhi. Fabrication and photocatalytic properties of novel ZnO/$ZnAl_2O_4$ nanocomposite with $ZnAl_2O_4$ dispersed inside ZnO network[J]. AIChE Journal, 2012, 58(2): 573-582.

[17] ABDERRAZEK K, NAJOUA F S, SRASRA E. Synthesis and characterization of [Zn-Al] LDH: Study of the effect of calcination on the photocatalytic activity[J]. Applied Clay Science, 2016, 119: 229-235.

[18] WANG Xiao-rong, WU Ping-xiao, HUANG Zhu-jian, ZHU Neng-wu, WU Jian-hua, LI Ping, DANG Zhi. Solar photocatalytic degradation of methylene blue by mixed metal oxide catalysts derived from ZnAlTi layered double hydroxides[J]. Applied Clay Science, 2014, 95: 95-103.

[19] AHMED A A A, TALIB Z A, BIN-HUSSEIN M Z, ZAKARIA A, ALLOY J. Improvement of the crystallinity and photocatalytic property of zinc oxide as calcination product of Zn-Al layered double hydroxide [J]. Journal of Alloys and Compounds, 2012, 539: 154-160.

[20] ZHANG Li, YAN Jian-hui, ZHOU Min-jie, YANG Ya-hui, LIU You-nian. Fabrication and photocatalytic properties of spheres-in-spheres ZnO/$ZnAl_2O_4$ composite hollow microspheres[J]. Applied Surface Science, 2013, 268: 237-245.

[21] PARHI P, MANIVANNAN V. Microwave metathetic approach for the synthesis and characterization of $ZnCr_2O_4$[J]. Journal of the European Ceramic Society, 2008, 28(8): 1665-1670.

[22] TAN Da-zhi, FAN Wen-jie, XIONG Wan-nan, SUN Han-xue, LI An, DENG Wei-qiao. Study on adsorption performance of conjugated microporous polymers for hydrogen and organic solvents: The role of pore volume[J]. European Polymer Journal, 2012, 48(4): 705-711.

[23] CHENG Xiang, HUANG Xin-rui, WANG Xing-zu, SUN De-zhi. Influence of calcination on the adsorptive removal of phosphate by Zn-Al layered double hydroxides from excess sludge liquor [J]. Journal of Hazardous Materials, 2010, 177(1): 516-523.

[24] IGUCHI S, TERAMURA K, HOSOKAWA S, TANAKA T. Photocatalytic conversion of CO_2 in an aqueous solution using various kinds of layered double hydroxides[J]. Catalysis Today, 2015, 251: 140-144.

[25] XIA Sheng-jie, LIU Feng-xian, Ni Zhe-ming, XUE Ji-long, QIAN Ping-ping. Layered double hydroxides as efficient photocatalysts for visible-light degradation of Rhodamine B[J]. Journal of colloid and interface science, 2013, 405: 195-200.

[26] KAWAMURA S, PUSCASU M C, YOSHIDA Y, IZUMI Y. Tailoring assemblies of plasmonic silver/gold and zinc–gallium layered double hydroxides for photocatalytic conversion of carbon dioxide using UV–visible light[J]. Applied Catalysis A: General, 2015, 504: 238-247.

[27] SONG Gui-xian, XIN Feng, CHEN Jing-shuai, YIN Xiao-hong. Photocatalytic reduction of CO_2 in cyclohexanol on CdS-TiO_2 heterostructured photocatalyst[J]. Applied Catalysis A: General, 2014, 473: 90-95.

[28] OHNO T, HIGO T, MURAKAMI N, SAITO H, ZHANG Qi-tao, YANG Yin, TSUBOTA T. Photocatalytic reduction of CO_2 over exposed-crystal-face-controlled TiO_2 nanorod having a brookite phase with co-catalyst loading[J]. Applied Catalysis B: Environmental, 2014, 152: 309-316.

[29] IGUCHI S, TERAMURA K, HOSOKAWA S, TANAKA T. Effect of the chloride ion as a hole scavenger on the photocatalytic conversion of CO_2 in an aqueous solution over Ni-Al layered double hydroxides[J]. Physical Chemistry Chemical Physics, 2015, 17(27): 17995-18003.

[30] LEE D S, CHEN H J, CHEN Yu-wen. Photocatalytic reduction of carbon dioxide with water using $InNbO_4$ catalyst with NiO and Co_3O_4 cocatalysts[J]. Journal of Physics and Chemistry of Solids, 2012, 73(5): 661-669.

Citation: *L. ZHANG et al., "Synthesis of Composite Oxides Derived from Zn-Ni-Al Layered Double Hydroxides and its Use in Photocatalytic Reduction of CO2", International Journal of Advanced Research in Chemical Science (IJARCS), vol. 4, no. 4, p. 10, 2017. http://dx.doi.org/10.20431/2349-0403.0404001*